WHIRL FLUTTER PREDICTIONS FOR DISTRIBUTED TILTROTOR CONFIGURATIONS

Seyhan Gul
Science and Technology Corporation
Ames Research Center, Moffett Field, CA, USA

Hyeonsoo Yeo
U.S. Army Combat Capabilities Development Command
Aviation & Missile Center
Ames Research Center, Moffett Field, CA, USA

ABSTRACT

A family of generic hingeless hub distributed tiltrotor configurations was modeled in RCAS and studied for whirl flutter. Also modeled was a baseline conventional configuration for comparison. A sensitivity study was carried out using the baseline model to provide a fundamental understanding. Wing torsion and rotor flap stiffness significantly impacted the instability speed. Reducing wing beam stiffness stabilized the system due to lower participation of wing torsion motion in this mode. Various distributed tiltrotor configurations were analyzed. Adding a same-size rotor to 40% wing span only slightly decreased the instability speed. On the other hand, utilizing two small rotors with half the disk area greatly stabilized the system. Placing these rotors at the wing tip in a coaxial configuration is also beneficial, but not as much as distributing them over the wing. Hence, eVTOL configurations appear to exhibit better stability characteristics than traditional tiltrotor aircraft; however, analysis for a real aircraft is necessary. Impact of rotor-rotor and rotor-wing aerodynamic interactions was studied using Viscous Vortex Particle Method (VVPM). Predictions show that the effect of rotor wake on the wing may be important if wing beam is the unstable mode.

NOTATION

b	span, ft
c	chord, ft
EA	axial stiffness, lbf
EI_{beam}	beam stiffness, lbf·ft^2
EI_{chord}	chord stiffness, lbf·ft^2
GJ	torsion stiffness, lbf·ft^2
km_y	radius of gyration in chord direction, ft
km_z	radius of gyration in thickness direction, ft
r	radial position, ft
R	blade radius, ft
θ_{75}	collective, deg
V	speed, knots
x	span position, ft

Presented at 49th European Rotorcraft Forum, Bückeburg, Germany, September 5–7, 2023.

INTRODUCTION

Tiltrotor aircraft may encounter whirl flutter at high cruise speeds in airplane mode. Typically, thick and stiff wings are used to push the stability boundary, which has a significant impact on parasitic drag. This is one of the major barriers to achieving higher speeds with rotary-wing aircraft.

Whirl flutter has been of interest to rotorcraft engineers for more than 60 years. Various model- and full-scale tests have been conducted, starting with the full-scale XV-3 aircraft in 1957 (Ref. 1). Some of the notable wind tunnel tests are full-scale Bell Model 300 (XV-15 rotor; gimballed hub; Refs. 2, 3), Wing and Rotor Aeroelastic Test System (WRATS; U.S. Army/NASA/Bell; 1/5 Froude-scaled V-22; gimballed hub; Ref. 4), full-scale Boeing Model 222 (soft in-plane hingeless hub; Ref. 5), TiltRotor Aeroelastic Stability Testbed (TRAST; U.S. Army; gimballed and hingeless hubs; Ref. 6), Maryland Tiltrotor Rig (MTR; University of Maryland; gimballed and hingeless hubs;

Ref. 7), and Advanced Testbed for TILtrotor Aeroelastics (ATTILA; Netherlands Aerospace Centre; gimballed hub; Ref. 8). TRAST, MTR, and ATTILA are active test programs. In addition to the test efforts, important analytical work has also been carried out. These are listed reverse-chronologically as Refs. 9–28.

Although significant progress has been made, maximum cruise speed of modern tiltrotor aircraft is still near 300 knots. Moreover, test and analysis efforts have focused primarily on the conventional tiltrotor configuration of the V-22 (Fig. 1), which has a single rotor mounted at the wing tip on either side of the fuselage. Due to recent developments in battery and electric motor technology, many new configurations have started to emerge. These are named as eVTOL (electric Vertical Take-Off and Landing) aircraft and they typically rely on distributed electric propulsion for safety through redundancy. Most of the designs employ multiple rotors/propellers mounted on the wings. After vertical take-off, much like a conventional tiltrotor aircraft, some or all of the rotors tilt and airplane mode flight is achieved. Some of the notable designs are Joby S4 (Fig. 2a; Ref. 29), Kitty Hawk Heaviside 2 (Fig. 2b), Archer Midnight (Fig. 2c; Ref. 30), Wisk Generation 6 (Fig. 2d; Ref. 31), Airbus Vahana (Fig. 2e), and Vertical Aerospace VX4 (Fig. 2f).

Figure 1: Bell Boeing V-22 Osprey

Despite the recent developments, the literature on whirl flutter investigation for these new configurations is limited to Refs. 32–34. Although some in-house analysis may have been performed by the designers with the knowledge gained kept proprietary, eVTOL whirl flutter characteristics are not widely understood. This paper aims to address this gap by studying airplane mode stability of various distributed tiltrotor configurations. A family of generic hingeless configurations was systematically modeled in RCAS (Rotorcraft Comprehensive Analysis System; Refs. 35,36). Sensitivity of stability to wing and rotor stiffness was investigated. Impact of rotor-rotor and rotor-wing aerodynamic interactions was studied using Viscous Vortex Particle Method (VVPM; Ref. 37). The objective is to guide future designers by using a generic tiltrotor model. Simplicity was one of the key objectives to ease reproduction of results by future researchers.

MATHEMATICAL MODEL

The first step of the current work was to create a generic hingeless tiltrotor model. Aeroelastic properties of distributed tiltrotor configurations are not available in the public domain, which presented a challenge for modeling a realistic aircraft that shows pertinent stability behavior. On the other hand, academia and government publish details of their test rigs to support technology development. The Maryland Tiltrotor Rig was an excellent starting point for this generic model because of the availability of the properties and wind tunnel test data, which provided validation data for the analysis (Ref. 38). The models built in this work are not geometrically similar to MTR, but the same airfoils were used for the rotor and wing together with a similar pylon mass. The stiffness of the rotor blades were also scaled from MTR.

Four hingeless configurations were developed, each a semi-span model of the right wing/pylon. Configuration 1 (baseline; Fig. 3a) utilizes a 4-ft radius rotor mounted at the wing tip. This represents a conventional tiltrotor aircraft. Configuration 2 (Fig. 3b) has 2×4-ft radius rotors—one at the wing tip and the other at 40% span. This was built to study the impact of an additional rotor. Configuration 3 is similar to Configuration 2, except the rotors are smaller. These were scaled down to 2.83-ft radius to operate at the same disk loading as the full-size rotor of Configuration 1 (scaling factor is $\sqrt{0.5} = 0.707$ for half the disk area assuming aircraft drag is the same). Dynamic Mach scaling laws were used to preserve the tip Mach number and non-dimensional rotor frequencies. Pylon mass was also reduced considering the lower power requirements of a smaller rotor. Configuration 4 (Fig. 3d) uses the same small rotors as Configuration 3—except this time both the rotors are placed at the wing tip. Co- and counter-rotating cases were analyzed for Configurations 2–4 to study the impact of gyroscopic moments. All the rotors turn counter-clockwise for the co-rotating cases whereas the second rotor (placed at 40% span for Configurations 2 and 3 and at wing trailing edge for Configuration 4) turns clockwise for the counter-rotating cases.

(a) Joby S4

(b) Kitty Hawk Heaviside 2

(c) Archer Midnight

(d) Wisk Generation 6

(e) Airbus Vahana

(f) Vertical Aerospace VX4

Figure 2: Notable eVTOL configurations

Each rotor blade was modeled with 20 nonlinear beam elements and 18 aerodynamic segments. A pitch bearing was modeled at 5%R which was actuated for pitch control. Uniform inflow was used for all calculations except the aerodynamic interactions study. Linear unsteady terms were included. C81 airfoil tables were used for VR-7 airfoil (Ref. 12). Gravity was neglected as it is not significant. Principal characteristics of the baseline 4-ft and small 2.83-ft radius rotors are given in Table 1. Blade sectional properties are given in Table 2. The values for the small rotor are given in parenthesis where they differ from the baseline. Fanplots for the baseline and small rotors are given in Figs. 4a and 4b. The rotors exhibit the same natural frequencies at their corresponding operating rotor speeds due to the dynamic Mach scaling. Torsion mode is not visible on the fan plots as the stiffness was kept high for simplicity.

The wing was modeled with 10 nonlinear beam elements and 20 aerodynamic segments. Uniform cross-sectional properties were used. Each pylon was modeled as a rigid

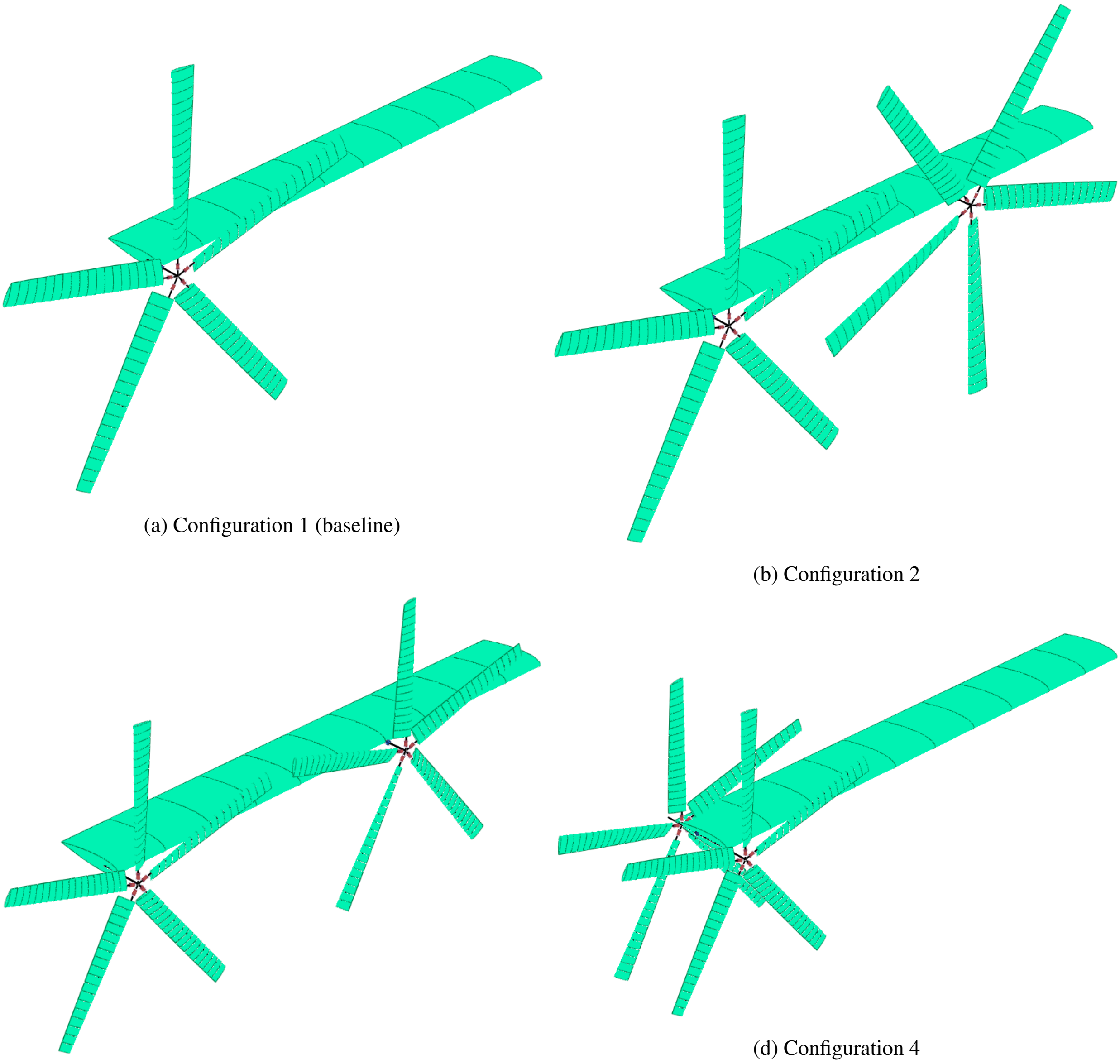

(a) Configuration 1 (baseline)

(b) Configuration 2

(c) Configuration 3

(d) Configuration 4

Figure 3: Configurations analyzed

bar. Uniform inflow was used for all predictions except the aerodynamic interactions study. C81 airfoil tables were used for NACA0018 airfoil (Ref. 12). Principal characteristics of the wing/pylon are given in Table 3. The values in parenthesis are for Configurations 3 and 4 as the pylon inertia is scaled down due to the lower power requirements of the smaller rotors. The pylon length and c.g. are relative to wing quarter chord. The frequencies are for Configuration 1 without the rotor mass (only wing and pylon). Note that although the dimensions are comparable to a real eVTOL aircraft, a structural analysis was not carried out for the components. The wing/pylon frequencies are typical of a conventional tiltrotor aircraft.

BASELINE STABILITY

First, a trim solution was obtained for freewheeling condition. Freewheeling results in similar collective as powered flight which influences flap-lag coupling. The trim variable for a given rotor and tunnel speed is the collective angle and the trim target is zero torque at the rotor hub. Figure 5 shows freewheeling collective predictions with respect to flight speed. Sea level atmospheric conditions were used. A high collective is required for high-speed axial flight. Note that collective does not change between the configurations due to the Mach scaling.

After trim, coupled system equations were linearized for the stability solution. Constant coefficient approach was

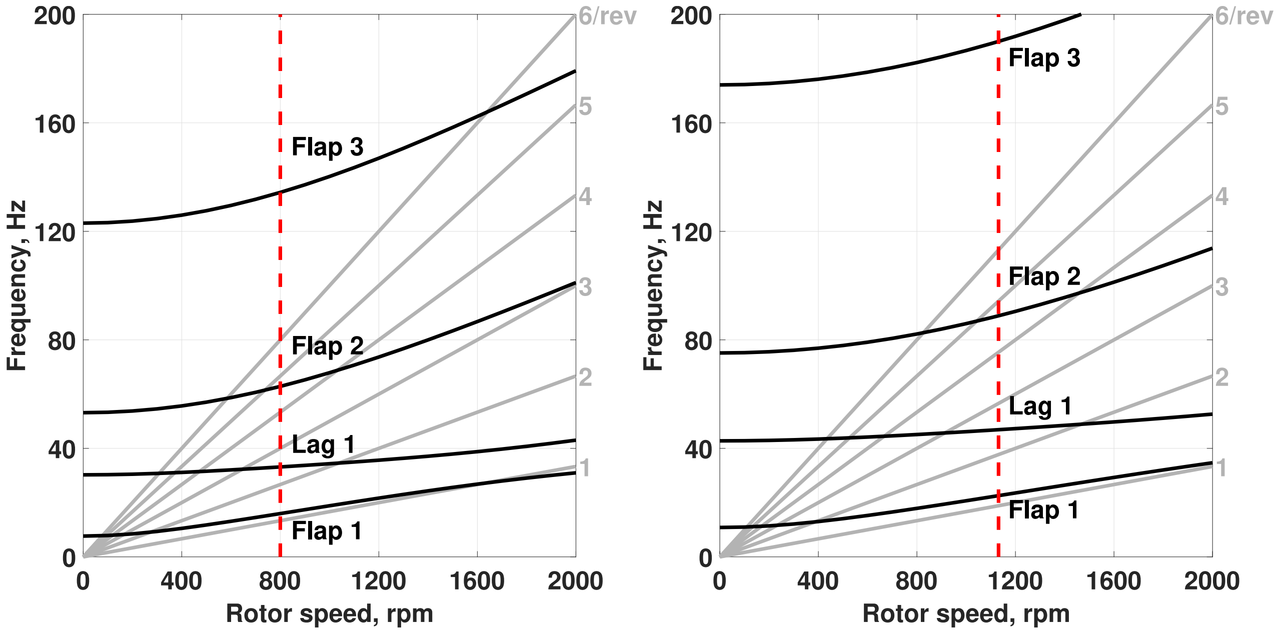

(a) Baseline rotor (4-ft radius)

(b) Small rotor (2.83-ft radius)

Figure 4: Fanplots for baseline and small rotors (vacuum, $\theta_{75} = 0°$)

Table 1: Principal characteristics of the baseline and small rotors (in parenthesis)

Number of blades	5
Radius	4 ft (2.83 ft)
Chord	0.444 ft (0.314 ft)
Aspect ratio	9
Solidity	0.177
Rotor speed	800 rpm (1131.4 rpm)
Cruise tip Mach number	0.3
Precone	2°
Hub	Hingeless
First flap frequency	1.20/rev
First lag frequency	2.49/rev
Twist	-37°
Airfoil	VR-7 (tab=0°)
Root cutout	10%R
Structural damping	1%

used as it is appropriate for axial flight. Using the system mass, damping, and stiffness matrices, eigenvalues were obtained by RCAS, which result in frequency and damping values for the coupled system. This is also called eigenanalysis. Rotor speed perturbations were not allowed due to the assumed electric drive. The assumption is that the electric motor can control the rotor speed sufficiently. Figure 6 shows frequency and damping predictions with respect to flight speed for Configuration 1 (baseline). Only the primary modes are shown. The naming convention shows the dominant motion for coupled modes. Regressive lag mode is the second regressive mode ($\zeta - 2$) due to

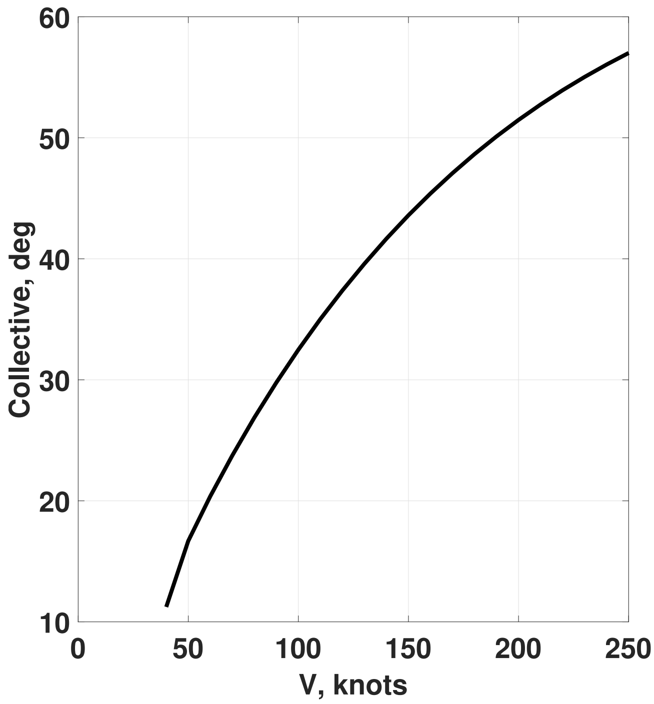

Figure 5: Change of freewheeling collective with respect to flight speed

5 blades. Wing beam mode frequency shows a slight decrease with speed, chord frequency is constant, and torsion frequency first decreases and then stays constant at higher speeds. On the other hand, rotor regressive flap frequency changes and interacts with wing beam, chord and torsion modes at different speeds. Interaction with the wing beam mode occurs around 150 knots (Fig. 6a) which results in

Table 2: Blade sectional properties of the baseline and small rotors (in parenthesis)

r/R	Mass, slug/ft	EI_{beam}, lbf·ft^2	EI_{chord}, lbf·ft^2	GJ, lbf·ft^2	EA, lbf	km_y, ft	km_z, ft
0.000	0.02 (0.01)	10^9	10^9	10^5 (25000)	10^9	0.04444 (0.03142)	0
0.050	0.02 (0.01)	10^9	10^9	10^5 (25000)	10^9	0.04444 (0.03142)	0
0.051	0.02 (0.01)	800 (200)	16000 (4000)	10^5 (25000)	10^9	0.04444 (0.03142)	0
0.350	0.02 (0.01)	800 (200)	16000 (4000)	10^5 (25000)	10^9	0.04444 (0.03142)	0
0.351	0.02 (0.01)	700 (175)	16000 (4000)	10^5 (25000)	10^9	0.04444 (0.03142)	0
1.000	0.02 (0.01)	700 (175)	16000 (4000)	10^5 (25000)	10^9	0.04444 (0.03142)	0

Table 3: Principal characteristics of wing and pylon

(Semi) span	10 ft
Chord	1.333 ft
Aspect ratio	7.5
Mass	0.2 slug/ft
EI_{beam}	65×10^4 lbf·ft^2
EI_{chord}	17×10^5 lbf·ft^2
GJ	68×10^3 lbf·ft^2
km_y	0.3333 ft
First beam frequency	4.31 Hz
First chord frequency	7.06 Hz
First torsion frequency	14.23 Hz
Airfoil	NACA 0018
Pylon length	0.8 ft
Pylon c.g.	0.4 ft
Pylon mass	2.18 slug (1.09 slug)
Pylon pitch/yaw moment of inertia	0.75 slug·ft^2 (0.375 slug·ft^2)

a sudden decrease in wing beam damping (Fig. 6b). The instability speed is 135 knots. Note that this is not a prediction for a real aircraft. The instability speed was intentionally kept low in this model in order to study the trends and make comparisons; it should not be evaluated in an absolute sense.

SENSITIVITY STUDY

A sensitivity study was carried out using Configuration 1 to provide a fundamental understanding of the physical phenomena. Wing beam, chord, and torsion stiffness and rotor flap and lag stiffness were varied, and the impact on stability was studied. Figure 7 shows the impact of wing beam stiffness on stability. The stiffness was changed by 25% to amplify its effect. Beam frequency shifts along with some small change in the torsion frequency (Fig. 7a). This is because beam and torsion motions are coupled due to high pylon mass and pylon c.g. offset. The interesting behavior here is that beam mode is more stable when the stiffness is lower (Fig. 7b). This is due to the change in the participation of beam and torsion motions in this mode. Figure 8 shows torsion participation in the beam mode shape. The magnitude is arbitrary and normalized for a 1-ft beam tip displacement. When the stiffness is increased, there is less beam displacement for the same torsion deformation, which means more torsion for the same beam displacement. This beam up—pitch up coupling destabilizes the system. Hence, designers must take care and consider couplings when stiffening the wing to avoid whirl flutter.

Figure 9 shows the impact of wing chord stiffness on stability. Only chord frequency changes. The chord mode is more stable when the stiffness is lower, but torsion damping decreases. This is again due to a change in how the motions are coupled, this time through gyroscopic moments. The stability behavior does not change; only shifts are observed in the damping values.

Figure 10 shows the impact of wing torsion stiffness on stability. As expected, a shift in the torsion frequency is observed. Beam damping decreases when the torsion stiffness is lower. The instability speed is reduced by 40 knots due to a 25% reduction in stiffness. On the other hand, a 25% increase stabilizes the beam mode and completely eliminates the instability up to 250+ knots. This is again due to the coupling of beam and torsion motions. It can be concluded that wing torsion motion is an important driver of whirl flutter. Therefore, torsion stiffness has a significant impact on the instability speed.

Figure 11 shows the combined impact of wing beam, chord, and torsion stiffness on stability. This is a more realistic change than changing the stiffness in individual directions. Damping for beam mode decreases and the instability speed reduces by 20 knots with a 25% decrease in stiffness. No significant change is observed for chord damping. Torsion damping reduces significantly at high speeds when the wing is softer.

Figure 12 shows the impact of rotor flap stiffness on stability. The flap frequency of the baseline model is 1.2/rev. Cases with 1.1/rev (53% reduction in flap stiffness for 5%R–35%R) and 1.3/rev (88% increase in flap stiffness for 5%R–35%R) were also studied. Regressive flap frequency

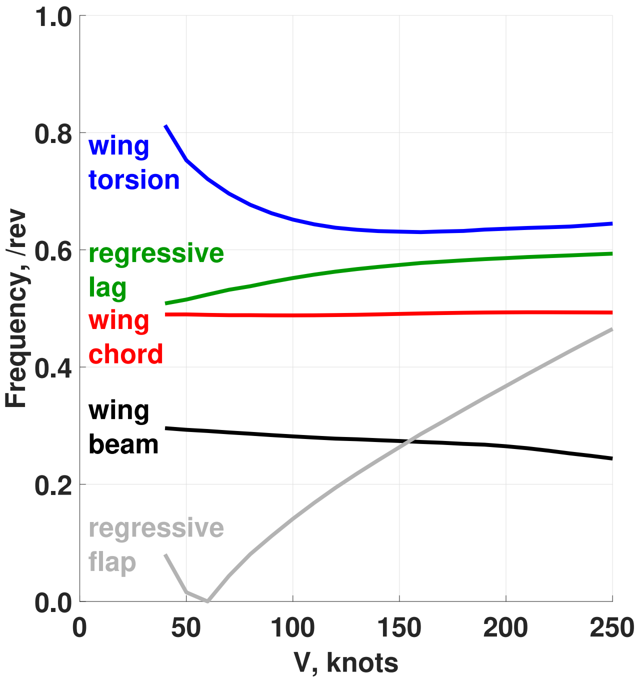

(a) Frequency

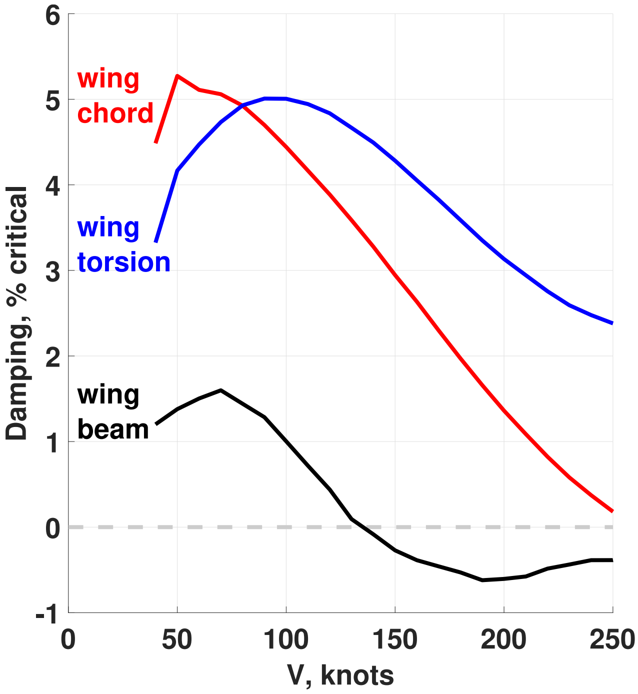

(b) Damping

Figure 6: Stability of Configuration 1 (baseline)

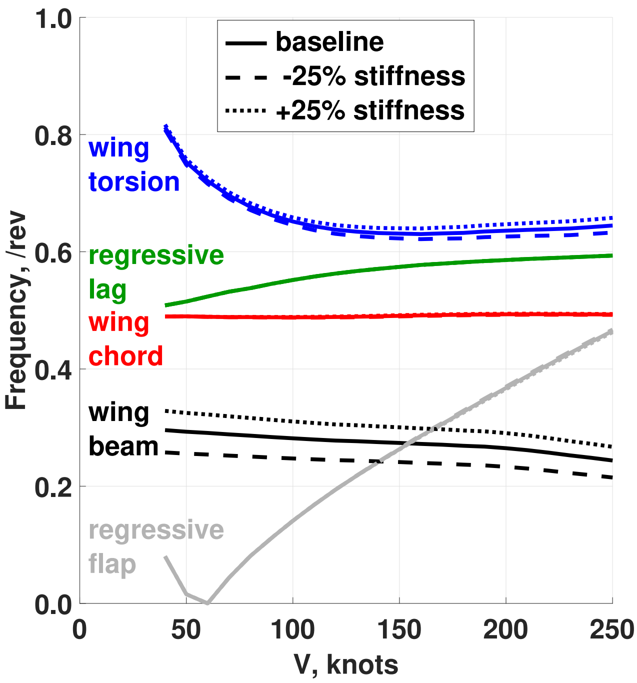

(a) Frequency

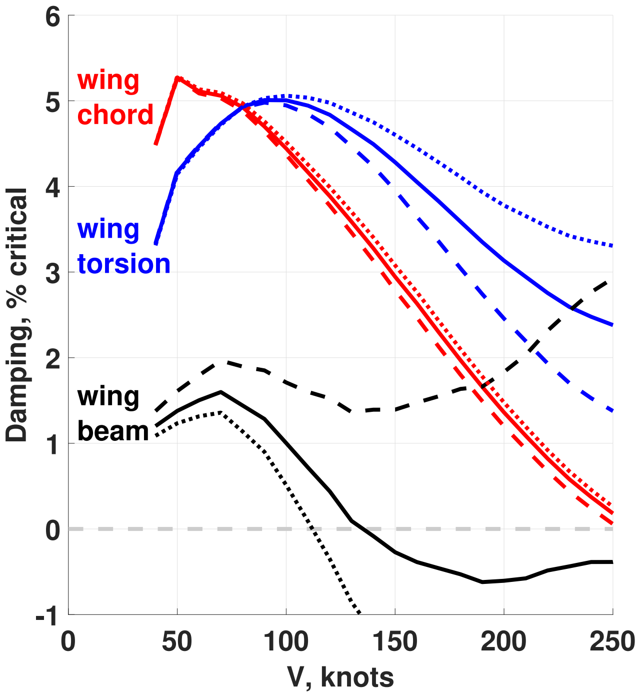

(b) Damping

Figure 7: Impact of wing beam stiffness on stability of Configuration 1 (baseline)

changes along with some change in the regressive lag frequency. This is due to the rotor flap-lag coupling that occurs for highly twisted blades or at high collective angles (Fig. 5). Wing beam and torsion damping are much lower when the flap frequency is 1.1/rev. The instability speed reduces by 60 knots. For the 1.3/rev flap frequency case, the instability disappears until around 235 knots (a 100-knots improvement). This shows that flap frequency is another major driving factor behind whirl flutter.

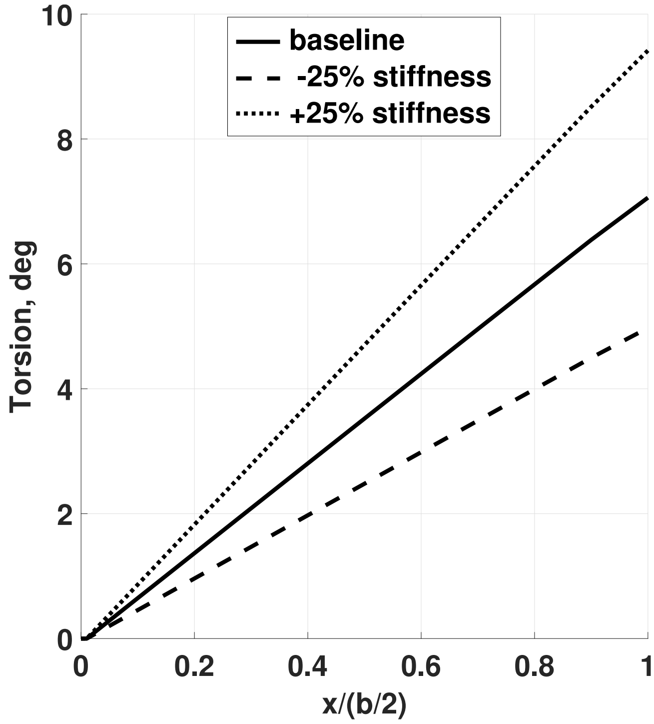

Figure 8: Torsion participation (positive pitch up) in beam mode shape for a 1-ft beam tip displacement

Figure 13 shows the impact of rotor lag stiffness. The baseline lag frequency is 2.49/rev. Frequencies of 1.66/rev (69% reduction in lag stiffness for 5%R–35%R) and 3.24/rev (275% increase in lag stiffness for 5%R–35%R) were studied. Wing torsion frequency and damping are affected due to coupling of wing and rotor motions. However, wing beam damping and the instability behavior appear to be relatively unaffected even with the large changes in stiffness. The instability speed for the 1.66/rev case is 125 knots, only 10 knots lower than the baseline.

STABILITY OF DISTRIBUTED TILTROTOR CONFIGURATIONS

Stability of various distributed tiltrotor configurations was analyzed and compared with Configuration 1 (baseline) which represents a traditional tiltrotor. Figure 14 compares the stability roots of Configurations 1 and 2. The only difference between them is the addition of the second rotor at 40% wing span, hence it is a useful comparison to provide a physical understanding. A second regressive flap mode appears due to the additional rotor. A reduction in the wing frequencies is observed due to the additional inertia. Torsion frequency is affected the most. Chord damping decreases if the rotors are co-rotating and slightly increases if they are counter-rotating. However, torsion damping reduces by more than 1% when the rotors counter-rotate. This is due to the change in the direction of gyroscopic moment. The damping trend does not change. Beam damping decreases with flight speed for both cases, and even though the interaction speed with the regressive flap mode is the same, the instability speed reduces from 135 knots to 115 knots (a 20-knots reduction) due to higher destabilizing aerodynamic loads. This is not a significant change considering the addition of a large rotor to the system.

Figure 15 shows a comparison between Configurations 1 and 3 which have similar thrust capability (same disk loading). The frequencies are normalized with the rotor speed of each configuration. Torsion frequency increases due to the distributed rotor/pylon mass (higher non-dimensional frequency despite the higher rotation speed). The regressive flap mode still interacts with the beam mode, but no reduction in the beam damping is observed. The instability disappears until 250+ knots where chord mode is expected to become unstable. Chord and torsion damping are lower at low speeds for Configuration 3, but this behavior is reversed at high speeds. No important difference is observed between co- and counter-rotating cases.

Figure 16 compares Configurations 1 and 4. Configuration 4 is special because the wing beam-torsion coupling disappears. This is because the net pylon c.g. is on the wing elastic axis. Similar to Configuration 3, the beam mode is stabilized. However, torsion damping decreases significantly and becomes critical at high speeds. The instability

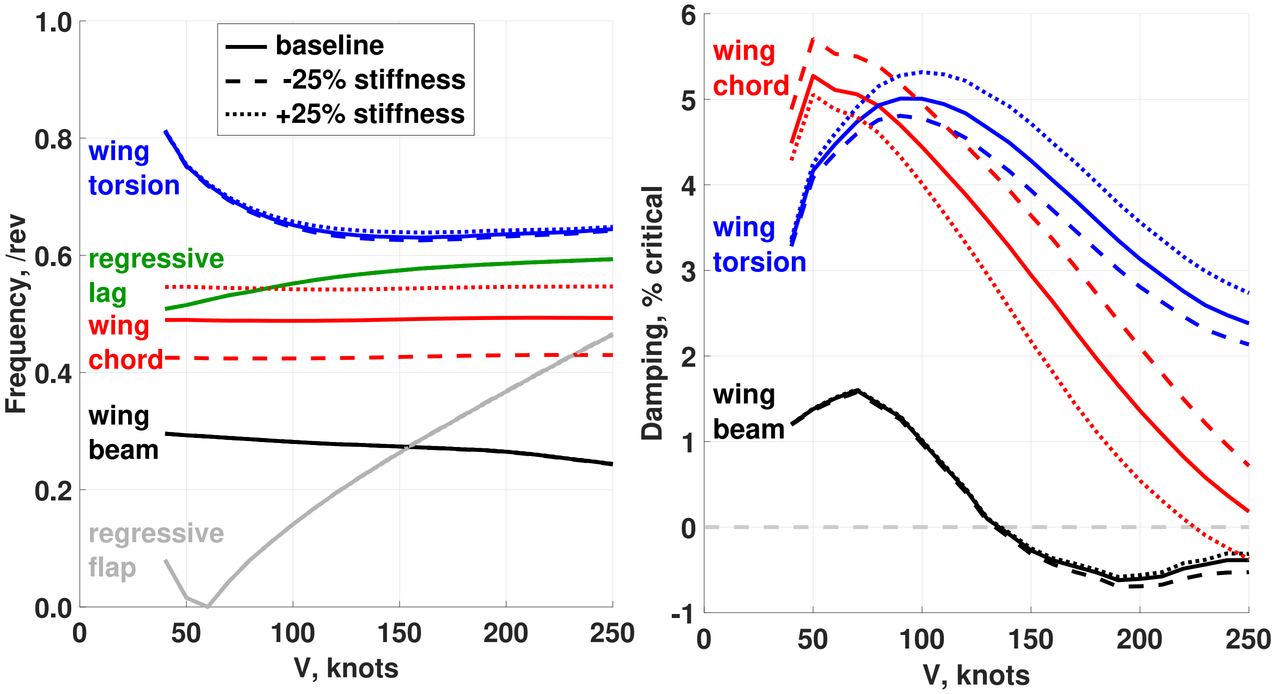

(a) Frequency

(b) Damping

Figure 9: Impact of wing chord stiffness on stability of Configuration 1 (baseline)

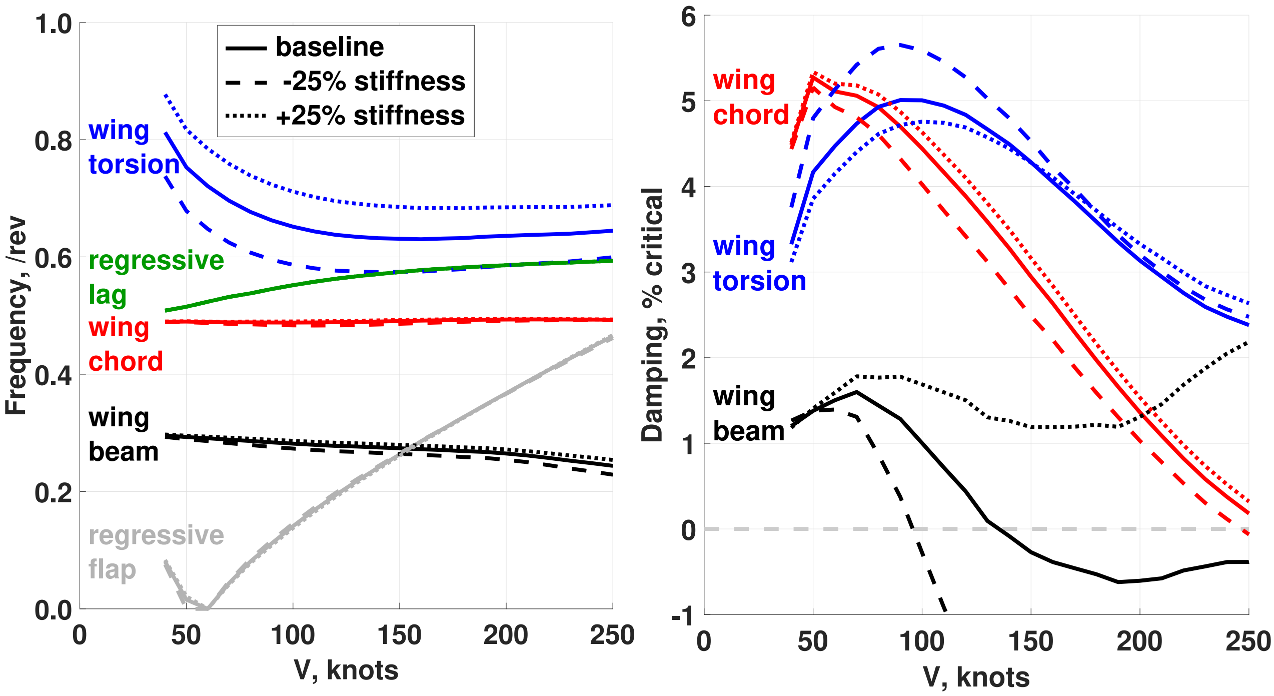

(a) Frequency

(b) Damping

Figure 10: Impact of wing torsion stiffness on stability of Configuration 1 (baseline)

disappears until 190 knots (a 55-knots improvement). The damping behavior is similar to the beam damping of Configuration 1. This shows that even though distributing the rotors on the wing (Configuration 3) is more stabilizing, a significant improvement is possible even with small, tip-mounted rotors compared to a single large rotor at the wing tip. The takeaway from this study is that eVTOL configurations can be expected to exhibit better stability characteristics than traditional tiltrotor aircraft, though analysis for a real aircraft is necessary.

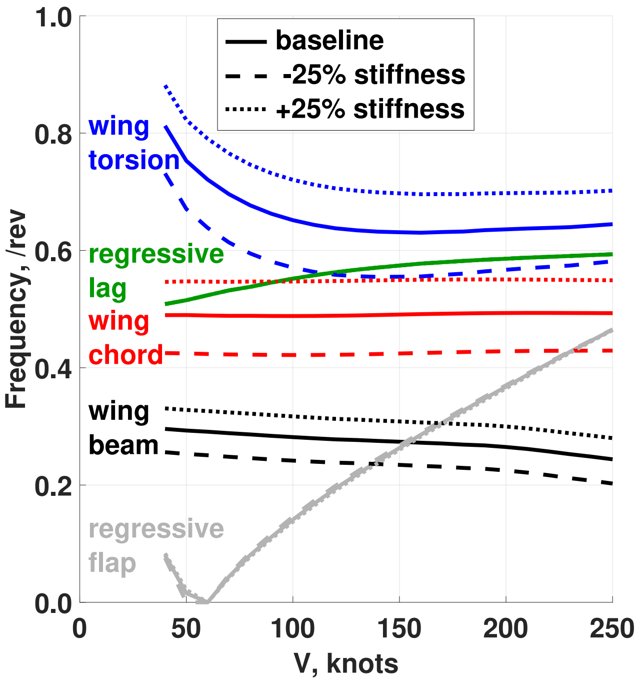

(a) Frequency

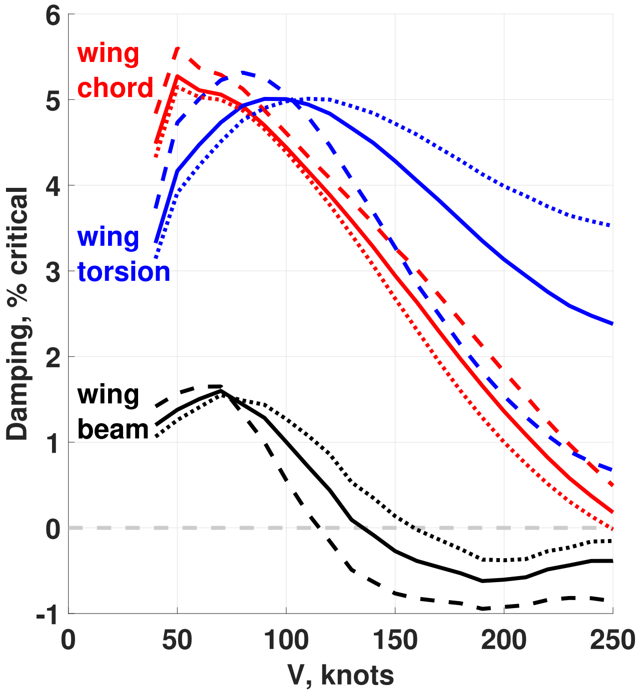

(b) Damping

Figure 11: Combined impact of wing stiffness on stability of Configuration 1 (baseline)

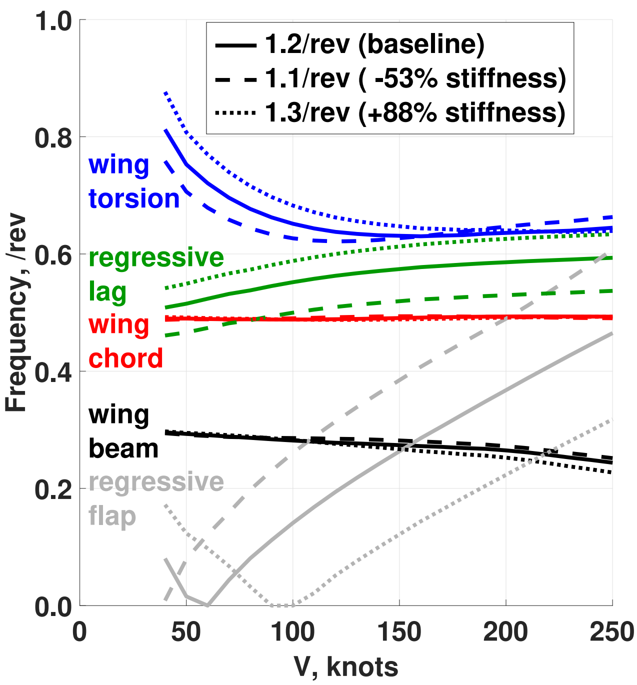

(a) Frequency

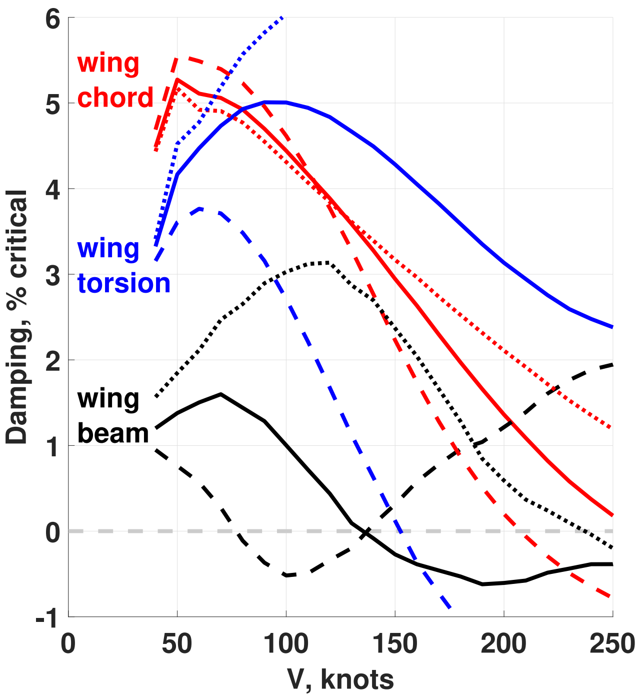

(b) Damping

Figure 12: Impact of rotor flap stiffness on stability of Configuration 1 (baseline)

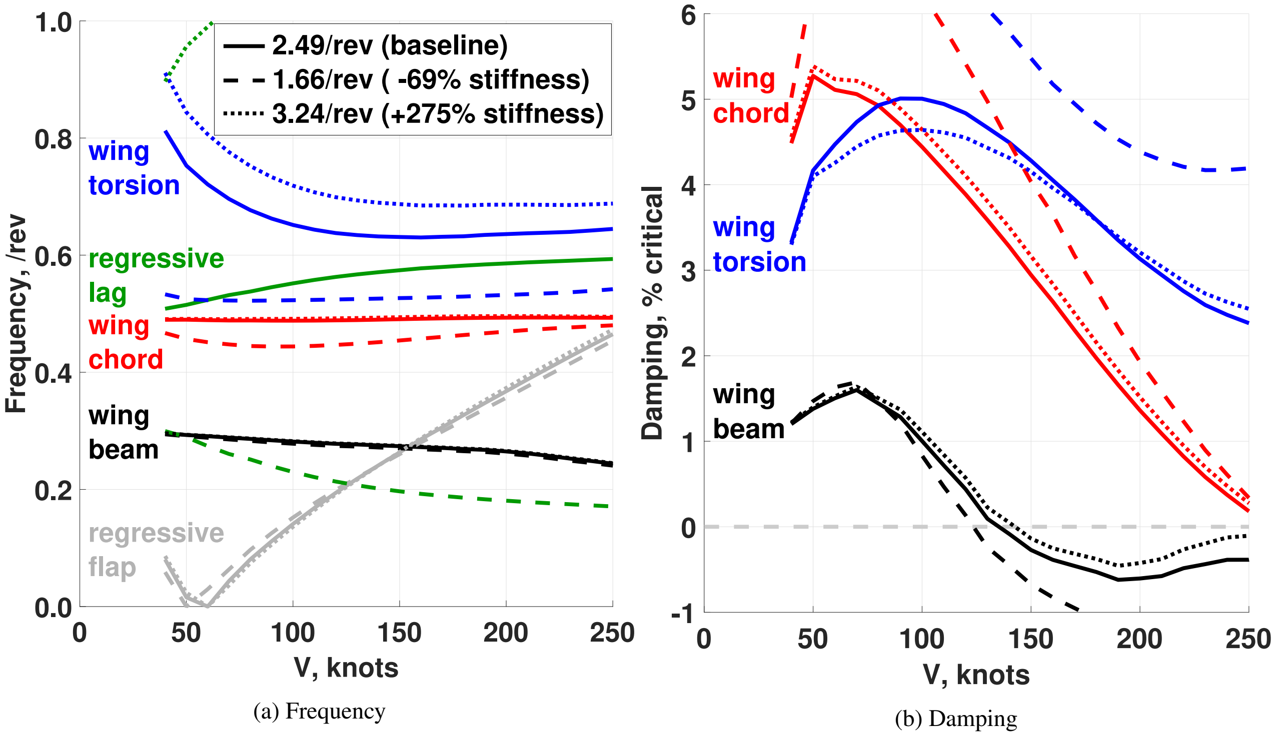

(a) Frequency

(b) Damping

Figure 13: Impact of rotor lag stiffness on stability of Configuration 1 (baseline)

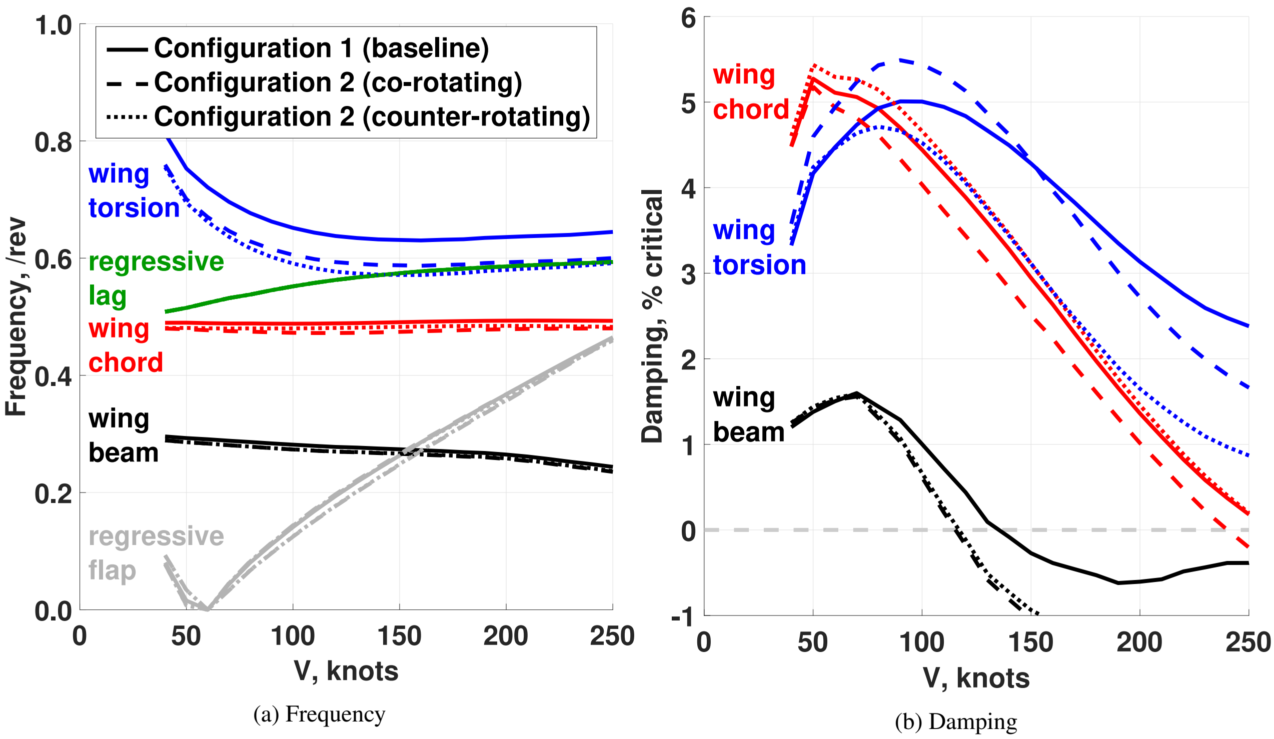

(a) Frequency

(b) Damping

Figure 14: Impact of number of rotors on stability (Configuration 1 versus 2)

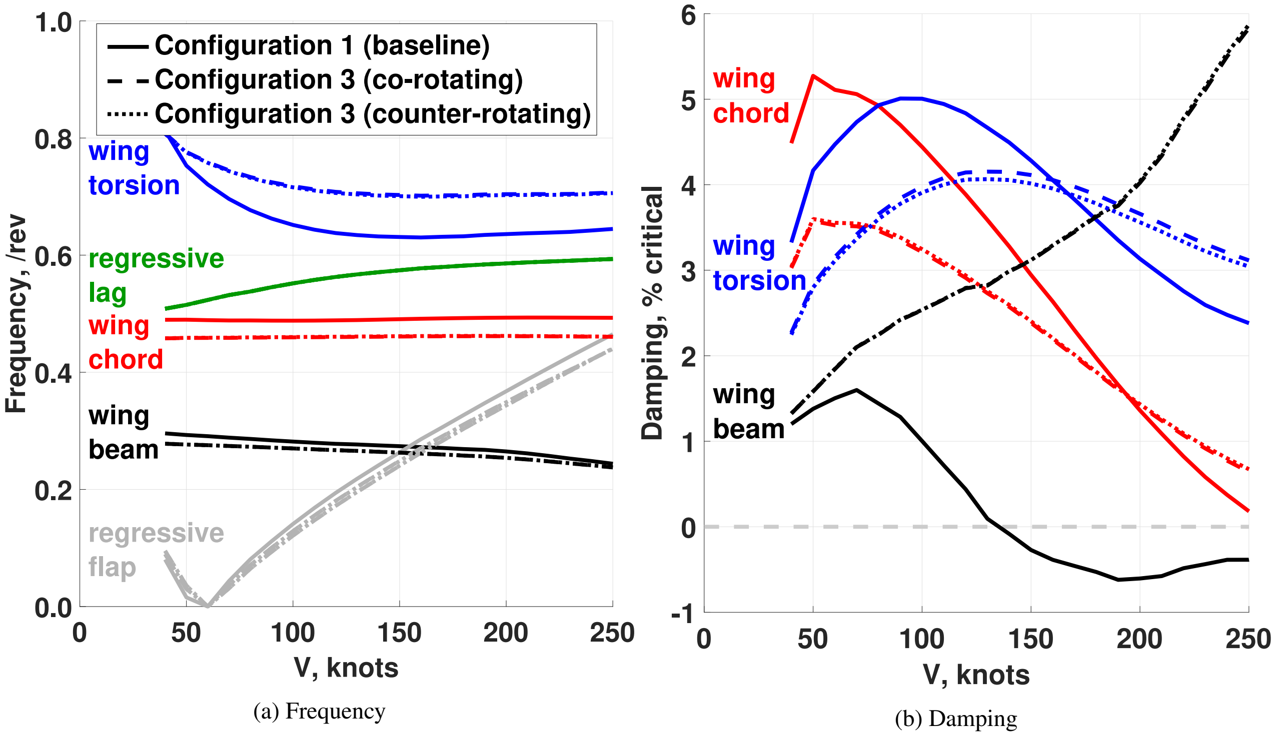

Figure 15: Impact of distributed rotors on stability (Configuration 1 versus 3)

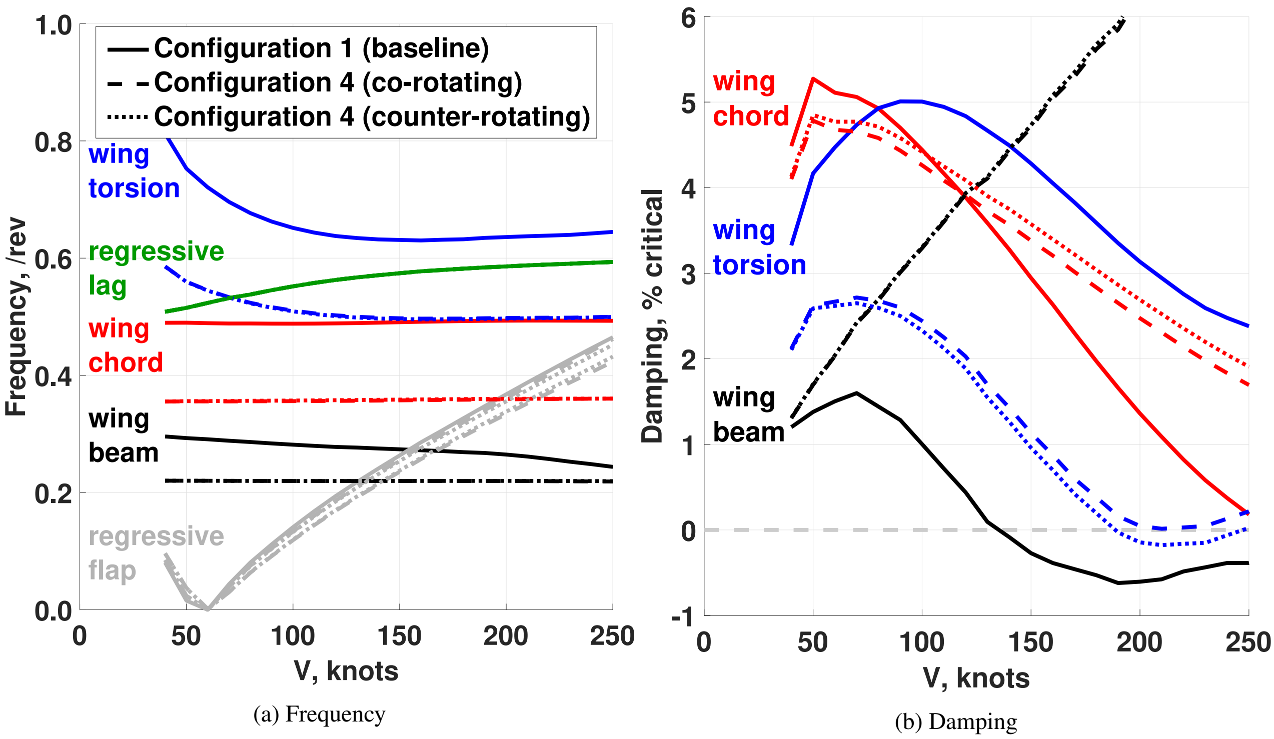

Figure 16: Impact of tip-mounted rotors on stability (Configuration 1 versus 4)

IMPACT OF AERODYNAMIC INTERACTIONS ON STABILITY

Aerodynamic interactions between the rotor and the wing is typically ignored in whirl flutter predictions. The assumption is that the wake is quickly washed away at high-speed axial flight, therefore the wake interactions are negligible. However, this has not yet been comprehensively examined and reported. Moreover, rotor-rotor and rotor-wing aerodynamic interactions may be important for stability of distributed tiltrotor configurations. At the very least, the effects need to be documented for future researchers/designers. In order to examine the impact of aerodynamic interactions, the Viscous Vortex Particle Method (VVPM) was used. VVPM solves the incompressible Navier-Stokes equation in a vorticity-velocity form with a grid-free Lagrangian representation.

The predictions reported so far have been obtained without any aerodynamic interactions. The eigenanalysis method was used where the system equations are linearized around a trim state and eigenvalues are calculated by RCAS using mass, damping, and stiffness matrices. VVPM cannot be used in conjunction with eigenanalysis because the states are not defined. Instead, transient perturbation method had to be used, which is nothing but simulation of a wind tunnel test. In this method, first, the trim solution is obtained in freewheeling condition just like the eigenanalysis method. Then, instead of linearization, the system is perturbed near the natural frequency of the wing mode of interest. The perturbation can either be due to a mechanical load or a collective/cyclic input to the rotor (stick-stir). In this case, a wing tip load (1 lbf for beam and chord modes and 10 lbf·ft for torsion mode) was used for direct excitation. After the wing starts vibrating at its resonant frequency, the perturbation is stopped and the decay of the wing root moments is recorded. Then, Prony or Moving-Block method (Refs. 39, 40) can be used to extract the frequency and damping. This procedure must be repeated for each mode separately.

It is useful to introduce the changes step by step to build confidence in the transient perturbation method before moving on to the VVPM analysis. Figures 17 and 18 show a comparison of eigenanalysis and transient perturbation predictions for Configurations 1 and 3. Only the counter-rotating case was analyzed for Configuration 3 as it is more representative of an actual aircraft. Both Prony and moving-block methods were implemented for the transient perturbation analysis. Uniform inflow was used as before. The frequency predictions are the same between the different methods. Prony and moving-block result in similar damping predictions; however, some small differences exist when compared to the eigenanalysis results. The differences appear to be higher at high speeds except for the wing chord mode. Further investigation is necessary to understand the causes of these small differences, but for now the results are close enough to carry out an investigation using VVPM.

Three sets of stability roots were calculated: 1. VVPM for the rotor(s), uniform inflow for the wing, 2. VVPM for the rotor(s); rotor induced inflow for the wing (wing does not contribute to the vortex field), 3. VVPM for the rotor(s) and the wing (full aerodynamic interactions). Configurations 1 and 3 were analyzed. A systematic comparison is provided below.

Figure 19 compares stability roots obtained with uniform inflow and VVPM for Configuration 1. The wing modes are separated to different sub-plots for ease of comparison. A frequency comparison is not included as no pertinent information can be drawn. All the predictions were obtained using the transient perturbation method coupled with Prony. Figure 19a shows that the damping behavior of the beam mode stays the same but shifts to higher speeds. As the model complexity increases, the instability speed moves to higher speeds. The change is about 25 knots with full interactions. This shows that the effect of rotor wake on the wing may be important for stability if beam is the unstable mode. Further investigation is required to study the causes of differences. The chord and torsion damping reduce at low speeds when VVPM is introduced for the rotor (red dashed lines in Figs. 19b and 19c). The difference in the chord mode vanishes at high speeds.

Figure 20 performs the same comparison for Configuration 3. Some small changes are observed for beam and torsion damping. Chord damping is lower at lower speeds but it appears that no rotor-wing aerodynamic interaction is necessary to capture this effect. This reduction largely disappears at higher speeds. In general, no significant change is observed in the damping behavior of this configuration, even though the flow field may be more complicated due to multiple rotors.

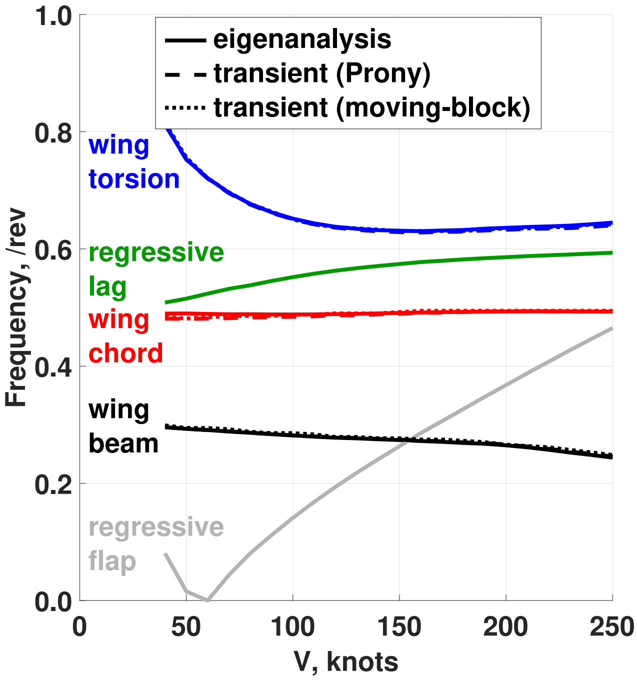

(a) Frequency

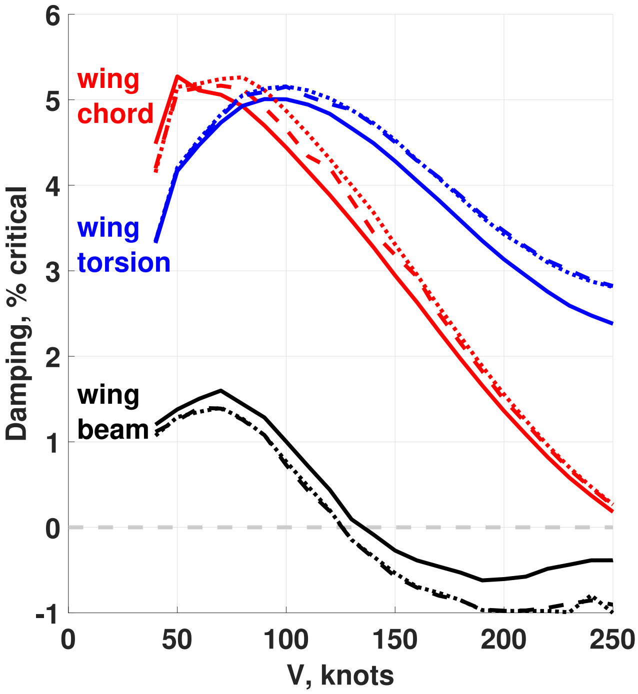

(b) Damping

Figure 17: Comparison of eigenanalysis and transient perturbation stability roots for Configuration 1 (baseline)

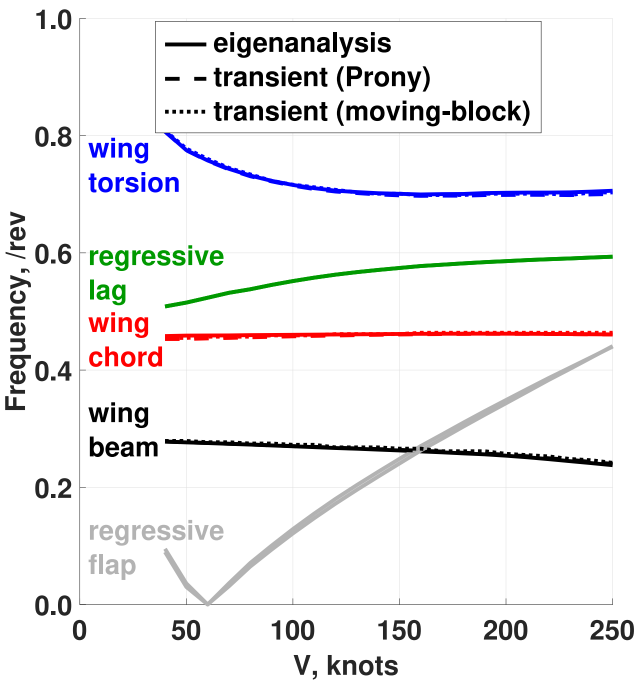

(a) Frequency

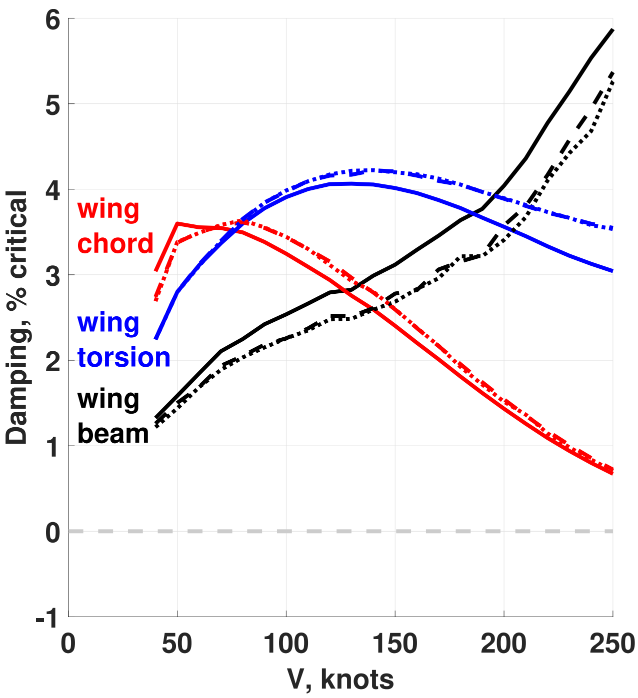

(b) Damping

Figure 18: Comparison of eigenanalysis and transient perturbation stability roots for Configuration 3 (counter-rotating)

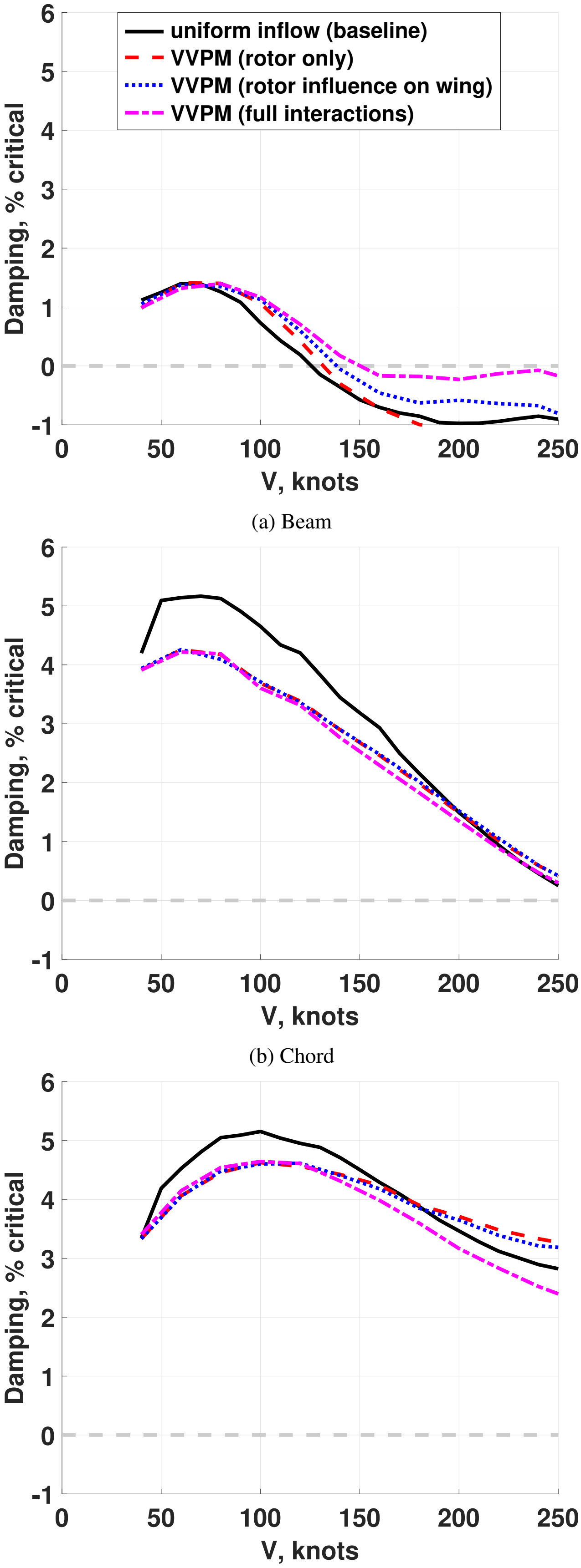

(a) Beam

(b) Chord

(c) Torsion

Figure 19: Impact of Viscous Vortex Particle Method on Stability for Configuration 1 (baseline)

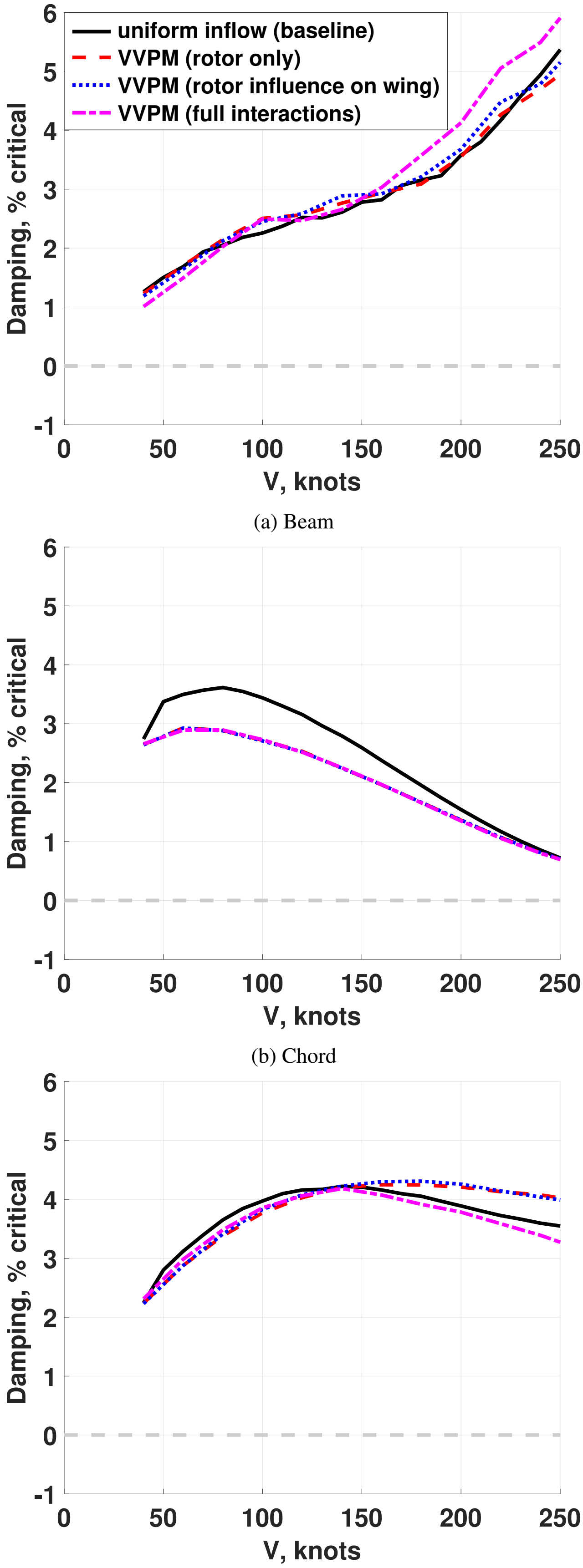

(a) Beam

(b) Chord

(c) Torsion

Figure 20: Impact of Viscous Vortex Particle Method on Stability for Configuration 3 (counter-rotating)

CONCLUSIONS

A family of generic hingeless hub distributed tiltrotor configurations was modeled in RCAS and analyzed for whirl flutter stability. Configurations with a single large rotor at the wing tip (baseline conventional), two distributed large rotors, two distributed small rotors, and two tip-mounted small rotors were analyzed. A sensitivity study was carried out for the baseline configuration by varying the wing and rotor stiffness. Rotor-wing and rotor-rotor aerodynamic interactions were modeled using Viscous Vortex Particle Method (VVPM). The key conclusions are as follows:

1. The instability speed for the baseline configuration is 135 knots. The instability occurs due to interaction of regressive flap mode with wing beam mode.

2. Adding a same-size rotor to 40% wing span decreased the instability speed from 135 knots to 115 knots (a 20-knots reduction). This is not a significant change considering the addition of a second large rotor.

3. The stability improved significantly when the large rotor at the wing tip was replaced by two small rotors with half the disk area (same disk loading). The instability behavior changed; wing beam is no longer the critical mode. The instability speed changed from 135 knots to 250+knots with distributed rotors over the wing and to 190 knots with tip-mounted rotors in a coaxial configuration. It appears that eVTOL configurations can be expected to exhibit better stability characteristics than traditional tiltrotor aircraft, though analysis for a real aircraft is necessary.

4. Modeling the rotor-wing aerodynamic interaction preserved the damping behavior for the conventional tiltrotor configuration but shifted the instability speed to higher values. The change is about 25 knots. It was shown that effect of rotor wake on the wing may be important if wing beam is the unstable mode. No significant change was observed for the distributed rotor configuration except chord damping at low speeds, which appears to be captured with VVPM on rotors only. Further investigation is necessary.

5. The sensitivity study for the baseline configuration shows that wing beam stiffness has a reverse impact on the instability speed; a higher beam stiffness results in a less stable system. This is due to participation of torsion motion in the beam mode. When the stiffness is increased, torsion participation increases (beam up—pitch up) which destabilizes the system.

6. Wing torsion and rotor flap stiffness have significant impact on stability. Increasing the torsion stiffness by 25% completely eliminated the instability until 250+ knots. Moving the rotor flap frequency from 1.2/rev to 1.3/rev also improved the stability and brought the instability speed to 235 knots (a 100-knots improvement).

REFERENCES

1. Maisel, M. D., Giulianetti, D. J., and Dugan, D. C., "The History of the XV-15 Tilt Rotor Research Aircraft: From Concept to Flight," NASA-SP-2000-4517, NASA, 2000.

2. Anon., "Advancement of Proprotor Technology. Task I: Design Study Summary," NASA-CR-114682, Bell Helicopter Company, September 1969.

3. Anon., "Advancement of Proprotor Technology. Task II: Wind-Tunnel Test Results," NASA-CR-114363, Bell Helicopter Company, September 1971.

4. Piatak, D. J., Kvaternik, R. G., Nixon, M. W., Langston, C. W., Singleton, J. D., Bennett, R. L., and Brown, R. K., "A Parametric Investigation of Whirl-Flutter Stability on the WRATS Tiltrotor Model," *Journal of the American Helicopter Society*, Vol. 47, (2), April 2002, pp. 134–144. DOI: https://doi.org/10.4050/JAHS.47.134

5. Magee, J. P., and Alexander, H. R., "Wind Tunnel Tests of a Full Scale Hingeless Prop/Rotor Designed for the Boeing Model 222 Tilt Rotor Aircraft," NASA-CR-114664, Boeing Vertol Company, October 1973.

6. Kreshock, A. R., Thornburgh, R. P., and Wilbur, M. L., "Overview of the TiltRotor Aeroelastic Stability Testbed," AIAA SciTech Forum, San Diego, California, January 2022.

7. Datta, A., Tsai, F., and Sutherland-Foggio, J., "Design of a New Tilt Rotor Test Facility at the University of Maryland," AIAA SciTech Forum, San Diego, California, January 2019.

8. van 't Hoff, S., van Vilsteren, J., Cocco, A., and Masarati, P., "Design of a Tiltrotor Semi-Span Wind Tunnel Model for Whirl Flutter Investigations," AIAA SciTech Forum, National Harbor, MD, January 2023.

9. Gul, S., and Datta, A., "Development of an Aeromechanics Solver for Loads and Stability of Hingeless Tiltrotors," *Journal of Aircraft*, Vol. 60, (1), January 2023, pp. 143–159. DOI: https://doi.org/10.2514/1.C036944

10. Gul, S., and Datta, A., "Aeroelastic Loads and Stability of Swept-Tip Hingeless Tiltrotors toward High-Speed Instability-Free Cruise," *Journal of the American Helicopter Society*, Vol. 68, (1), January 2023, pp. 1–18. DOI: https://doi.org/10.4050/JAHS.68.012001

11. Yeo, H., Kang, H., and Kreshock, A. R., "Unified Modeling of the TiltRotor Aeroelastic Stability Testbed for Proprotor Whirl Flutter," *Journal of Aircraft*, Vol. 60, (3), May 2023, pp. 1–13. DOI: https://doi.org/10.2514/1.C036950

12. Gul, S., and Datta, A., "Whirl Flutter Test of the Maryland Tiltrotor Rig: Prediction and Validation," AIAA SciTech Forum, San Diego, California, January 2022.

13. Yeo, H., and Kreshock, A. R., "Whirl Flutter Investigation of Hingeless Proprotors," *Journal of Aircraft*, Vol. 57, (4), July-August 2020, pp. 586–596. DOI: https://doi.org/10.2514/1.C035609

14. Kreshock, A. R., Thornburgh, R. P., and Yeo, H., "Comparison of Comprehensive Analyses Predicting Whirl Flutter Stability of the Wing and Rotor Aeroelastic Test System," *Journal of the American Helicopter Society*, Vol. 64, (4), October 2019, pp. 1–12. DOI: https://doi.org/10.4050/JAHS.64.042010

15. Yeo, H., Bosworth, J., Acree, C. W., Jr., and Kreshock, A. R., "Comparison of CAMRAD II and RCAS Predictions of Tiltrotor Aeroelastic Stability," *Journal of the American Helicopter Society*, Vol. 63, (2), April 2018, pp. 1–13. DOI: https://doi.org/10.4050/JAHS.63.022001

16. Acree, C. W., Jr., "Effects of V-22 Blade Modifications on Whirl Flutter and Loads," *Journal of the American Helicopter Society*, Vol. 50, (3), July 2005, pp. 269–278. DOI: https://doi.org/10.4050/1.3092863

17. Acree, C. W., Jr., Peyran, R. J., and Johnson, W., "Rotor Design Options for Improving XV-15 Whirl-Flutter Stability Margins," NASA-TP-2004-212262, NASA Ames Research Center, March 2004.

18. Srinivas, V., and Chopra, I., "Validation of a Comprehensive Aeroelastic Analysis for Tiltrotor Aircraft," *Journal of the American Helicopter Society*, Vol. 43, (4), October 1998, pp. 333–341. DOI: https://doi.org/10.4050/JAHS.43.333

19. Srinivas, V., Chopra, I., and Nixon, M. W., "Aeroelastic Analysis of Advanced Geometry Tiltrotor Aircraft," *Journal of the American Helicopter Society*, Vol. 43, (3), July 1998, pp. 212–221. DOI: https://doi.org/10.4050/JAHS.43.212

20. Barkai, S. M., and Rand, O., "The Influence of Composite Induced Couplings on Tiltrotor Whirl Flutter Stability," *Journal of the American Helicopter Society*, Vol. 43, (2), April 1998, pp. 133–145. DOI: https://doi.org/10.4050/JAHS.43.133

21. Acree, C. W., Jr., "An Improved CAMRAD Model for Aeroelastic Stability Analysis of the XV-15 with Advanced Technology Blades," NASA-TM-4448, NASA Ames Research Center, March 1993.

22. Popelka, D., Sheffler, M., and Bilger, J., "Correlation of Test and Analysis for the 1/5-Scale V-22 Aeroelastic Model," *Journal of the American Helicopter Society*, Vol. 32, (2), April 1987, pp. 21–33. DOI: https://doi.org/10.4050/JAHS.32.21

23. Johnson, W., Lau, B. H., and Bowles, J. V., "Calculated Performance, Stability, and Maneuverability of High-Speed Tilting-Prop-Rotor Aircraft," NASA-TM-88349, NASA Ames Research Center, September 1986.

24. Johnson, W., "Analytical Modeling Requirements for Tilting Proprotor Aircraft Dynamics," NASA-TN-D-8013, NASA Ames Research Center and U.S. Army Air Mobility R&D Laboratory, July 1975.

25. Johnson, W., "Dynamics of Tilting Proprotor Aircraft in Cruise Flight," NASA-TN-D-7677, NASA Ames Research Center and U.S. Army Air Mobility R&D Laboratory, May 1974.

26. Gaffey, T. M., "The Effect of Positive Pitch-flap Coupling (Negative δ_3) on Rotor Blade Motion Stability and Flapping," *Journal of the American Helicopter Society*, Vol. 14, (2), April 1969, pp. 49–67. DOI: https://doi.org/10.4050/JAHS.14.2.49

27. Young, M. I., and Lytwyn, R. T., "The Influence of Blade Flapping Restraint on the Dynamic Stability of Low Disk Loading Propeller-

Rotors," *Journal of the American Helicopter Society*, Vol. 12, (4), October 1967, pp. 38–54. DOI: https://doi.org/10.4050/JAHS.12.38

28. Hall, W. E., Jr., "Prop-Rotor Stability at High Advance Ratios," *Journal of the American Helicopter Society*, Vol. 11, (2), April 1966, pp. 11–26. DOI: https://doi.org/10.4050/JAHS.11.2.11

29. Stoll, A., and Bevirt, J., "Development of eVTOL Aircraft For Urban Air Mobility At Joby Aviation," Vertical Flight Society 78th Annual Forum, Fort Worth, Texas, May 2022.

30. Hirschberg, M., "Archer's Midnight Showing," *Vertiflite*, Vol. 69, (1), January/February 2023, pp. 54–59.

31. Gettinger, D., "Wisk 6th Gen Breaks Cover," *Vertiflite*, Vol. 68, (6), November/December 2022, pp. 26–27.

32. Castillo Capponi, D. I., *Multirotor Whirl Flutter: A semi-analytical approach*, Master's thesis, Delft University of Technology, 2022.

33. Liu Xu, V. Q., *Propeller-Wing Whirl Flutter: An analytical study*, Master's thesis, Delft University of Technology, 2020.

34. Hoover, C. B., Shen, J., Kreshock, A. R., Stanford, B., Piatak, D. J., and Heeg, J., "Whirl Flutter Stability and Its Influence on the Design of the Distributed Electric Propeller Aircraft X-57," 17th AIAA Aviation Technology, Integration, and Operations Conference, Denver, CO, June 2017.

35. Saberi, H., Khoshlahjeh, M., Ormiston, R. A., and Rutkowski, M. J., "Overview of RCAS and Application to Advanced Rotorcraft Problems," American Helicopter Society 4th Decennial Specialists' Conference on Aeromechanics, San Francisco, California, January 2004.

36. Saberi, H., Hasbun, M., Hong, J., Yeo, H., and Ormiston, R. A., "Overview of RCAS Capabilities, Validations, and Rotorcraft Applications," American Helicopter Society 71st Annual Forum, Virginia Beach, Virginia, May 2015.

37. He, C., and Zhao, J., "Modeling Rotor Wake Dynamics with Viscous Particle Method," *AIAA Journal*, Vol. 47, (4), April 2009, pp. 902–915. DOI: https://doi.org/10.2514/1.36466

38. Gul, S., and Yeo, H., "High-Speed Stability Predictions of Maryland Tiltrotor Rig and Parametric Study," Vertical Flight Society 79th Annual Forum, West Palm Beach, Florida, May 2023.

39. Tasker, F. A., and Chopra, I., "Assessment of Transient Analysis Techniques for Rotor Stability Testing," *Journal of the American Helicopter Society*, Vol. 35, (1), January 1990, pp. 39–50. DOI: https://doi.org/10.4050/JAHS.35.39

40. Bousman, W. G., and Winkler, D. J., "Application of the Moving-Block Analysis," AIAA Dynamics Specialists Conference, Atlanta, GA, April 1981.